Radio-Frequency Spectroscopy of Ultracold Fermions

S. Gupta,[1]* Z. Hadzibabic,[1] M. W. Zwierlein,[1] C. A. Stan,[1] K. Dieckmann,[1] C. H. Schunck,[1] E. G. M. van Kempen,[2] B. J. Verhaar,[2] W. Ketterle[1]

Radio-frequency techniques were used to study ultracold fermions. We observed the absence of mean-field "clock" shifts, the dominant source of systematic error in current atomic clocks based on bosonic atoms. This absence is a direct consequence of fermionic antisymmetry. Resonance shifts proportional to interaction strengths were observed in a three-level system. However, in the strongly interacting regime, these shifts became very small, reflecting the quantum unitarity limit and many-body effects. This insight into an interacting Fermi gas is relevant for the quest to observe superfluidity in this system.

Radio-frequency (RF) spectroscopy of ultracold atoms provides the standard of time. However, the resonance frequencies of ultracold atoms are sensitive to interactions between atoms, leading to the so-called clock shifts of the unperturbed resonances (*1*). These shifts limit the accuracy of current atomic clocks (*2*, *3*), but can also be used to characterize atomic interactions.

RF spectroscopy has previously been applied to cold atoms to determine the size and temperature of atom clouds (*4, 5*). RF methods have also been used for evaporative cooling, for preparing spinor Bose-Einstein condensates (BECs) (*6*, *7*), and as an output coupler for atom lasers (*5*, *8*). In all these experiments, shifts and broadenings due to atomic interactions were negligible. Recently, density-dependent frequency shifts of RF transitions were observed in rubidium (*9*) and sodium (*10*) BECs. These frequency shifts are proportional to the difference in mean-field energies of two internal atomic states and allow scattering lengths to be extracted. Mean-field shifts in BECs have also been observed by optical spectroscopy (*11*, *12*).

Here, we apply RF spectroscopy to ultracold clouds of fermions and demonstrate several phenomena: (i) the absence of a clock shift in a two-level system because of fermionic antisymmetry, (ii) the emergence of mean-field shifts in a three-level system after the relaxation of pair correlations, (iii) the limitation of mean-field shifts because of the unitarity limit, and (iv) the universality of the interaction energy in a dense cloud, independent of the attractive or repulsive nature of the two-particle interactions.

Research in ultracold fermions has advanced rapidly, with six groups now having cooled fermions into quantum degeneracy (*13*–*18*). A major goal of this research is to induce strong interactions by tuning magnetic fields to scattering resonances (called Feshbach resonances). Under these conditions, Cooper pairs of fermions may form, leading to superfluidity. This would establish a model system for studying Bardeen-Cooper-Schrieffer (BCS) pairing at densities nine orders of magnitude lower than in previous realizations in ^{3}He and superconductors. We show that RF spectroscopy can be used to characterize interactions between fermions in the regime where superfluidity has been predicted (*19*, *20*).

Our experimental technique for preparing ultracold fermions has been considerably improved since our earlier work (*17*, *21*). Because the Pauli exclusion principle suppresses elastic collisions between identical fermions at low temperatures and prevents evaporative cooling, we cooled fermionic ^{6}Li sympathetically with bosonic ^{23}Na loaded into the same magnetic trap. In contrast to previous work, we cooled both species in their upper hyperfine states (^{23}Na: $|F,m_F\rangle = |2,+2\rangle$, ^{6}Li: $|F,m_F\rangle = |3/2,+3/2\rangle$, where F and m_F are the quantum numbers for the total spin and its z component, respectively. This led to a reduction of inelastic loss processes and boosted our final fermion atom numbers by two orders of magnitude. We could produce BECs that contained up to 10 million sodium atoms in the $|2,+2\rangle$ state by evaporatively cooling pure bosonic samples in the magnetic trap. For a Bose-Fermi mixture, the finite heat capacity of the bosons limited the final lithium temperature after the 30-s evaporation cycle to $\sim 0.3\ T_F$ for 10 million fermions and $\sim T_F$ for 50 million fermions (*22*), where T_F is the Fermi temperature.

The spin states of ^{6}Li of most interest for superfluid pairing are the two lowest states $|1\rangle$ and $|2\rangle$ ($|1/2,+1/2\rangle$ and $|1/2,-1/2\rangle$ at low field), which are predicted to have an interstate s-wave (*23*) Feshbach resonance at $\sim$800 G (*24*, *25*). However, both states are high-field–seeking at these fields, which makes them unsuitable for magnetic trapping. We therefore transferred the atoms into an optical trap. For these experiments, 6 to 8 million $|3/2,+3/2\rangle$ lithium atoms were loaded into the optical trap at temperature $T \sim T_F \sim 35\ \mu$K (*26*). The atoms were then transferred to the lowest energy state $|1\rangle$, with an adiabatic frequency sweep around the lithium hyperfine splitting of 228 MHz. Magnetic fields of up to $\sim$900 G were applied, a range that encompasses the $|1\rangle - |2\rangle$ Feshbach resonance. Using RF-induced transitions near 80 MHz, we could create mixtures of states $|1\rangle$, $|2\rangle$, and $|3\rangle$ ($|3/2, -3/2\rangle$ at low field) and explore interactions between fermions in these states.

Collisions between atoms cause a shift of their energy, which is usually described by the mean-field effect of all the other atoms on the atom of interest. For example, atoms in state $|2\rangle$ experience an energy shift, $[(4\pi\hbar^2)/(m)]n_1a_{12}$, that is due to the presence of atoms in state $|1\rangle$. Here $\hbar$ is Planck's constant h divided by 2π, m is the mass of the atom, n_1 is the density of $|1\rangle$ atoms, and a_{12} is the interstate scattering length between states $|1\rangle$ and $|2\rangle$. We use the convention that positive scattering length corresponds to a repulsive interaction. Density-dependent shifts of the resonance frequency for the transition that connects two states have been observed in laser-cooled (*1*) and Bose-condensed (*9*, *10*) clouds.

In the case of ultracold fermions, only interactions between different internal states are allowed. For a system of density n, let us compare the energy of a gas prepared purely in state $|1\rangle$ to a gas in which one atom is transferred into state $|2\rangle$. The energy difference is $h\nu_{12} + [(4\pi\hbar^2)/(m)]na_{12}$, where ν_{12} is the resonance frequency of the noninteracting system. Similarly, the energy difference between a gas prepared purely in state $|2\rangle$ and a gas in which one atom is transferred into state $|1\rangle$ is $h\nu_{12} - [(4\pi\hbar^2)/(m)]na_{12}$.

However, these energy shifts should not affect the resonance for a coherent transfer out of a pure state. For fermions in the initial pure state, the pair-correlation function vanishes at zero distance because of the antisymmetry of the wave function. During any coherent transfer process, the state vectors of all the atoms rotate "in parallel" in Hilbert space; i.e., the superposition of the two spin states

[1]Department of Physics, Massachusetts Institute of Technology (MIT)–Harvard Center for Ultracold Atoms, and Research Laboratory of Electronics, MIT, Cambridge, MA 02139, USA. [2]Eindhoven University of Technology, Post Office Box 513, 5600 MB Eindhoven, Netherlands.

*To whom correspondence should be addressed. E-mail: deep@mit.edu

has the same relative phase for all atoms. Thus, the atoms remain identical and cannot interact in the *s*-wave regime. The mean-field energy is thus established only after the coherence of the superposition state is lost and the pair correlations have relaxed, forming a purely statistical mixture of the two states.

It is a consequence of Fermi statistics that spectroscopic methods do not measure the equilibrium energy difference between the initial and final state of the system, but rather measure the unperturbed resonance frequency. The expected absence of the clock shift has led to suggestions for the use of fermions in future atomic clocks (*27*). Our work presents an experimental demonstration of this phenomenon.

We determined the transition frequency between states $|1\rangle$ and $|2\rangle$, first starting with a pure state $|1\rangle$ and then with a pure state $|2\rangle$ sample. The absence of a splitting between these two lines proves the suppression of the clock shift. Fig. 1 shows an example of such measurements. The magnetic field was ramped up to 570 G with the cloud in state $|1\rangle$. At this field, $a_{12} \sim 150a_0$. Therefore, the expected equilibrium mean-field shifts were $\Delta\nu = \pm 5$ kHz for our mean density of 3×10^{13} cm^{-3} (*28*). The interaction between states $|1\rangle$ and $|2\rangle$ at this magnetic field was also observed in the mutual evaporative cooling of the two states in the optical trap. RF pulses 140 μs in duration were applied at frequencies near the unperturbed resonance $\nu_{12} \sim 76$ MHz. Atoms in states $|1\rangle$ and $|2\rangle$ could be monitored separately by absorption imaging, because they are optically resolved at this field. We observed a suppression of the clock shift by a factor of 30 (Fig. 1). Using the same method, we observed the absence of a clock shift at several other magnetic fields. In particular, we observed a suppression of more than three orders of magnitude at ~860 G (*29*).

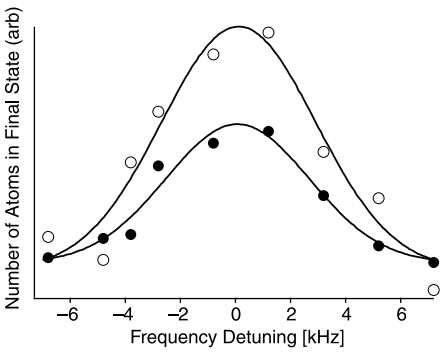

Fig. 1. Absence of the clock shift. RF transitions were driven between states $|1\rangle$ and $|2\rangle$ on a system prepared purely in state $|1\rangle$ (solid circles) and purely in state $|2\rangle$ (open circles). Mean-field interactions would have resulted in 5-kHz shifts for the two curves in opposite directions. Gaussian fits (solid lines) to the data are separated by 0.04 ± 0.35 kHz. This gives a clock-shift suppression factor of 30. Arb., arbitrary units.

P-wave interactions (*23*) could lead to a nonvanishing clock shift. However, at these low temperatures, they are proportional to T or T_F, whichever is higher, and are therefore strongly suppressed.

We can observe mean-field shifts and scattering lengths spectroscopically by driving transitions from a statistical mixture of two states to a third energy level. [While this work was in progress, use of a similar method to measure scattering lengths in fermionic ^{40}K was reported (*30*).] Specifically, we recorded the difference between the RF spectra for the $|2\rangle \rightarrow |3\rangle$ transition in the presence and in the absence of state $|1\rangle$ atoms. The presence of atoms in state $|1\rangle$ is then expected to shift the resonance by (*31*).

$$\Delta\nu = \frac{2\hbar}{m} n_1(a_{13} - a_{12}) \qquad (1)$$

In our experimental scheme to determine the interaction energy at different magnetic fields (Fig. 2), the system was prepared by ramping up the magnetic field to 500 G with the atoms in state $|1\rangle$. Either partial or complete RF transfer to state $|2\rangle$ was then performed. The number of atoms in state $|1\rangle$ was controlled by adjusting the speed of a frequency sweep around the $|1\rangle \rightarrow |2\rangle$ resonance. A fast, nonadiabatic sweep created a superposition of the two states, whereas a slow, adiabatic sweep prepared the sample purely in state $|2\rangle$. A wait time of 200 ms was allowed for the coherence between states $|1\rangle$ and $|2\rangle$ to decay and the system to equilibrate.

Typical parameters for the decohered $|1\rangle - |2\rangle$ mixture were mean-density $n_1 \sim 2.4 \times 10^{13}$ cm^{-3} and $T \sim 0.7\ T_F$. The magnetic field was then changed to the desired value, and the transition from state $|2\rangle$ to state $|3\rangle$ was driven with 140-μs RF pulses (Fig. 2C). We monitored the appearance of atoms in state $|3\rangle$ and the disappearance of atoms from state $|2\rangle$, using simultaneous absorption imaging. Fig. 2D shows the unperturbed and perturbed resonances at the magnetic field $B = 480$ G. The position of the unperturbed resonance

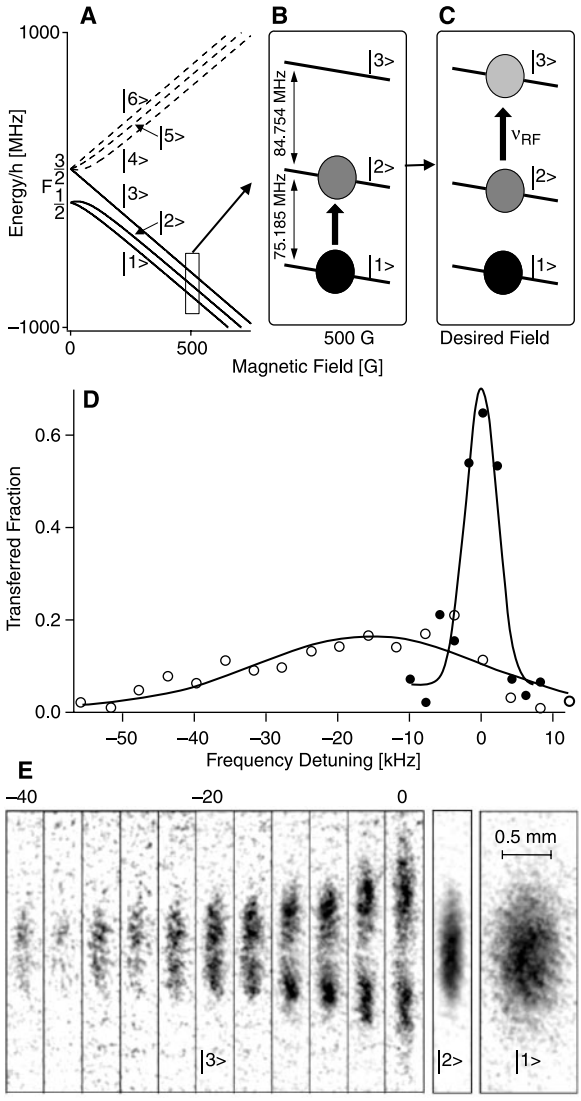

Fig. 2. Schematic of the mean-field measurement and representative spectra at 480 G. (**A**) Hyperfine structure of the ground state of ^{6}Li. (**B** and **C**) Experimental scheme: (B) Preparation of a mixture of atoms in states $|1\rangle$ and $|2\rangle$, and (C) RF spectroscopy of the $|2\rangle \rightarrow |3\rangle$ transition using a variable radio frequency (ν_{RF}). (**D**) The fraction of atoms transferred from $|2\rangle$ to $|3\rangle$, with $|1\rangle$ atoms absent (solid circles) and present (open circles). The mean-field shift is computed from Gaussian fits to the data (solid lines). (**E**) Spatial images of state $|3\rangle$ for the perturbed resonance. The optical trap was turned off immediately after the RF pulse and absorption images of the atoms were taken after 120 μs of expansion time. The central section of ~150-μm vertical extent was used to extract the transferred fractions in (D). (E) also shows images of states $|2\rangle$ and $|1\rangle$ for zero RF detuning. States $|3\rangle$ and $|2\rangle$ were imaged simultaneously to observe their complementary spatial structure. State $|1\rangle$ was imaged after 760 μs of expansion time to record its density for normalization purposes.

ν_{23} also determines the magnetic field to an accuracy of <0.1 G. Fig. 2E shows absorption images of atoms in state $|3\rangle$, obtained for different values of the applied radio frequency. One can clearly see the spatial dependence and thus the density dependence of the mean-field shift: Close to the unperturbed resonance, the low-density wings of the cloud are predominantly transferred, whereas the high-density central part of the cloud is transferred only at sufficient detuning. To suppress spurious effects from this spatial dependence, only a small central part of the images was used to extract the transferred atomic fraction.

To ensure that our mean-field measurements were performed on a statistical mixture, we measured the time scale for decoherence in our system. The decay of the $|1\rangle - |2\rangle$ coherence at 500 G was observed by monitoring the $|2\rangle \rightarrow |3\rangle$ transfer at the measured unperturbed resonance ν_{23}, as a function of wait time (Fig. 3). For wait times that are small compared to the decoherence time of the $|1\rangle - |2\rangle$ superposition, the $|2\rangle \rightarrow |3\rangle$ RF drive places each atom in an identical three-state superposition. All mean-field shifts are then absent and the resulting transfer is unchanged from the unperturbed case. For longer wait times, the $|1\rangle - |2\rangle$ superposition decoheres and mean-field interactions set in. This shifts the resonance frequency of the $|2\rangle \rightarrow |3\rangle$ transition, reducing the transferred fraction at ν_{23}. The measured decoherence time of $\sim$12 ms was attributed mainly to the sensitivity of ν_{12} to magnetic field variations across the cloud. These inhomogeneities cause the relative phase of the $|1\rangle - |2\rangle$ superposition in different parts of the trap to evolve at different rates, given by the local ν_{12}. Atoms that travel along different paths within the trap therefore acquire different phases between their $|1\rangle$ and $|2\rangle$ components. Being no longer in identical states, *s*-wave interactions between them are allowed. The inhomogeneities scale with B, whereas the sensitivity of the transition scales with $\partial\nu_{12}/\partial B$. We would thus expect the decoherence time to vary inversely with the product of these two quantities. Our hypothesis is supported by our observation of longer decoherence times at higher fields, where $B \times \partial\nu_{12}/\partial B$ is lower.

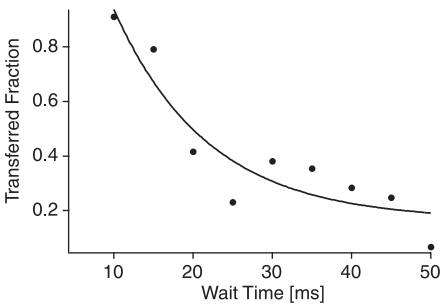

Fig. 3. Emergence of mean-field shifts due to decoherence at 500 G. Decoherence leads to a reduction of the $|2\rangle \rightarrow |3\rangle$ transfer at the unperturbed resonance ν_{23}. An exponential fit to the data (solid line) gives a time constant of 12 ms.

Fig. 4A summarizes the results of our mean-field measurements for a wide range of magnetic fields up to 750 G. For magnetic fields up to 630 G, our data can be explained fairly well by using Eq. 1 with the theoretical calculations of the scattering lengths shown in Fig. 4B and an effective density of $n_1 = 2.2 \times 10^{13}$ cm^{-3}, which is consistent with the initial preparation of the system at 500 G. A narrow resonance of a_{12} at $\sim$550 G (*21*, *25*, *32*) is indicated by the data but was not fully resolved. We also see additional structure near 470 G, which is not predicted by theory and deserves further study.

For fields above 630 G, the measured shifts strongly deviated from the predictions of Eq. 1, indicating a different regime of interactions. In the region between 630 G and 680 G, the two scattering lengths are expected to be large and positive, with $a_{13} \gg a_{12}$ (Fig. 4B). Eq. 1 would thus predict large positive mean-field shifts. In contrast, we observe very small shifts, indicating almost perfect cancellation of the two contributions. We also observe essentially no mean-field shifts between 680 G and 750 G, where the two scattering lengths are predicted to be very large in magnitude and of opposite signs, and in a simple picture should add up to a huge negative shift. These results are evidence for phenomena in a strongly interacting system, where the scattering length becomes comparable to either the inverse wave vector of interacting particles or the interatomic separation.

Eq. 1 is valid only for low energies and weak interactions, where the relative wave vector of the two particles, k, satisfies $k \ll 1/|a|$. For arbitrary values of ka, the s-wave interaction between two atoms is described by replacing the scattering length a with the complex scattering amplitude f.

$$f = \frac{-a}{1+k^2a^2}(1-ika) \qquad (2)$$

The real part of f, $\mathrm{Re}(f)$ determines energy shifts, and hence the ground state properties of an interacting many-body system. The imaginary part, $\mathrm{Im}(f)$ determines the (inverse) lifetime for elastic scattering out of a momentum state, and hence the dynamic properties of the system such as thermalization rates. For $k|a| \rightarrow \infty$, the elastic cross-section $\sigma = 4\pi\mathrm{Im}(f)/k$ monotonically approaches the well known "unitarity-limited" value of $4\pi/k^2$. On the other hand, the two-particle contribution to the mean-field energy, proportional to $-\mathrm{Re}(f) = a/(1 + k^2a^2)$ peaks at $|a| = 1/k$ and then, counterintuitively, decreases as $1/|a|$ for increasing $|a|$. Averaging $\mathrm{Re}(f)$ over a zero-temperature Fermi distribution with Fermi momentum $\hbar k_F$ limits its absolute value to $1.05/k_F$ and markedly weakens its dependence on the exact value of a in the $k_F|a| > 1$ regime (*33*). This results in a prediction for the mean-field energy that is sensitive to the sign of the scattering length, remains finite for $k_F|a| \gg 1$, and never exceeds $0.45\ E_F$, where E_F is the Fermi energy. Hence,

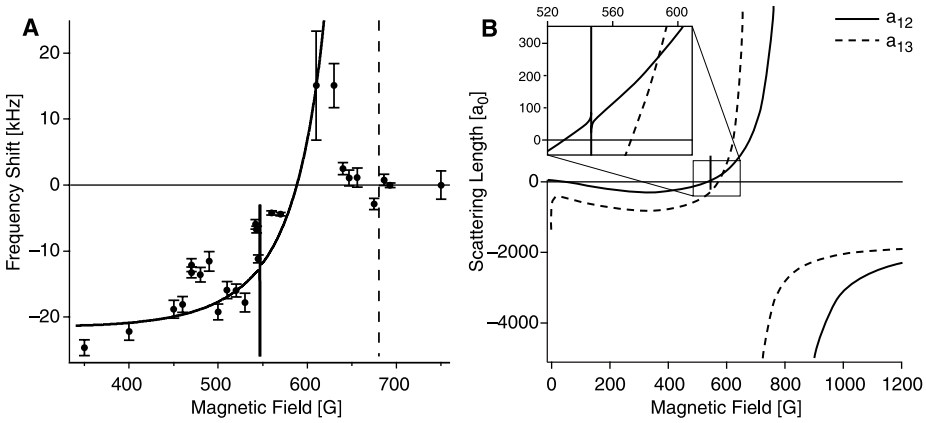

Fig. 4. Spectroscopic measurement of interaction energy. (**A**) Frequency shift versus magnetic field for the $|2\rangle \rightarrow |3\rangle$ resonance due to atoms in state $|1\rangle$. The shifts are computed by monitoring the arrival fraction in state $|3\rangle$ for 140-μs RF pulses, except at 750 G. At 750 G, because of strong inelastic losses between $|3\rangle$ and $|1\rangle$ atoms, we monitored the loss of atoms in state $|2\rangle$ after applying RF sweeps 3 ms in duration and 2 kHz in width. All the data points are normalized to the same atom number in state $|1\rangle$. The fit at low fields (solid line) uses Eq. 1 with $n_1 = 2.2 \times 10^{13}$ cm^{-3} and the theoretical calculations of the scattering lengths. The error bars reflect uncertainty in the state $|1\rangle$ atom number and the uncertainty in the Gaussian fits to the spectra. The dashed line indicates the position of the predicted a_{13} resonance. (**B**) *S*-wave scattering lengths a_{12} and a_{13} as a function of magnetic field, obtained from a highly model-independent quantum-scattering calculation. The calculation makes use of the presently available ^{6}Li experimental data (*40*) in a coupled channel approach to deduce accumulated phases that characterize the less well-known, short-range parts of the ^{6}Li + ^{6}Li scattering potential (*32*). a_{12} has a narrow Feshbach resonance at 550 G and a wide one at 810 G. a_{13} has a wide Feshbach resonance at 680 G.

this approach could qualitatively explain our results in the 630 to 680 G region, but it is in clear contradiction with negligible resonance shifts in the 680 to 750 G region (*34*).

We suggest that these discrepancies might be due to the fact that we are in the high-density regime, where $n|a|^3$ approaches unity. In a degenerate Fermi gas, the interparticle spacing is comparable to the inverse Fermi wave vector, $k_F^3 = 6\pi^2 n$. Hence, the unitarity limit coincides with the breakdown of the low-density approximation ($n|a|^3 \ll 1$) and higher order many-body effects can become important. Some recent many-body calculations (*35*–*37*) suggest that in the regime $k_F|a| \gg 1$ (or $n|a|^3 \gg 1$), the interaction energy is always negative and independent of both sign and magnitude of a. This suggests that whenever the scattering length is large, either positive or negative, the interaction energy is a universal fraction of the Fermi energy (*33*). This is a possible explanation for the small line shifts that we observed for fields higher than 630 G, where the interactions are strong in both states.

This picture is consistent with other recent experimental observations (*30*, *33*, *38*, *39*). Expansion energy measurements in a mixture of states $|1\rangle$ and $|2\rangle$ of ^{6}Li (*39*) showed a negative interaction energy at 720 G, which is on the repulsive side of the predicted Feshbach resonance. RF spectroscopy in ^{40}K (*30*) has also shown some saturation of the mean field in the vicinity of a Feshbach resonance, which may reflect the unitarity limit.

In characterizing an interacting Fermi gas by RF spectroscopy, we have demonstrated absence of clock shifts in a two-level system and introduced a three-level method for measuring mean-field shifts. For strong interactions, we have found only small line shifts that may reflect both the unitarity limit of binary collisions and many-body effects. It would be very important to distinguish between two-body and many-body effects by studying the gas over a broad range of temperatures and densities. In a very dilute and very cold gas, the weakly interacting limit could be extended to very large values of $|a|$, thus allowing for direct verification of molecular calculations. This presents experimental challenges, because cooling changes the density and the temperature together. It would also be interesting to study similar phenomena in bosonic gases, in order to distinguish to what extent the high density many-body effects depend on quantum statistics. This insight into the physics of strongly interacting Fermi gases must be taken into account in the search for superfluidity in these systems.

References and Notes

1. K. Gibble, S. Chu, *Phys. Rev. Lett.* **70**, 1771 (1993).
2. C. Fertig, K. Gibble, *Phys. Rev. Lett.* **85**, 1622 (2000).
3. Y. Sortais *et al.*, *Phys. Scr.* **T95**, 50 (2001).
4. A. G. Martin, K. Helmerson, V. S. Bagnato, G. P. Lafyatis, D. E. Pritchard, *Phys. Rev. Lett.* **61**, 2431 (1988).
5. I. Bloch, T. W. Hänsch, T. Esslinger, *Phys. Rev. Lett.* **82**, 3008 (1999).
6. M. R. Matthews *et al.*, *Phys. Rev. Lett.* **81**, 243 (1998).
7. J. Stenger *et al.*, *Nature* **396**, 345 (1998).
8. M.-O. Mewes *et al.*, *Phys. Rev. Lett.* **78**, 582 (1997).
9. D. M. Harber, H. J. Lewandowski, J. M. McGuirk, E. A. Cornell, *Phys. Rev. A.* **66**, 053616 (2002).
10. A. Görlitz *et al.*, *Phys. Rev. Lett.* **90**, 090401 (2003).
11. T. C. Killian *et al.*, *Phys. Rev. Lett.* **81**, 3807 (1998).
12. J. Stenger *et al.*, *Phys. Rev. Lett.* **82**, 4569 (1999).
13. B. DeMarco, D. S. Jin, *Science* **285**, 1703 (1999).
14. A. G. Truscott, K. E. Strecker, W. I. McAlexander, G. B. Partridge, R. G. Hulet, *Science* **291**, 2570 (2001).
15. F. Schreck *et al.*, *Phys. Rev. Lett.* **87**, 080403 (2001).
16. S. R. Granade, M. E. Gehm, K. M. O'Hara, J. E. Thomas, *Phys. Rev. Lett.* **88**, 120405 (2002).
17. Z. Hadzibabic *et al.*, *Phys. Rev. Lett.* **88**, 160401 (2002).
18. G. Roati, F. Riboli, G. Modungo, M. Inguscio, *Phys. Rev. Lett.* **89**, 150403 (2002).
19. M. Houbiers, H. T. C. Stoof, *Phys. Rev. A.* **59**, 1556 (1999).
20. M. Holland, S. J. J. M. F. Kokkelmans, M. L. Chiofalo, R. Walser, *Phys. Rev. Lett.* **87**, 120406 (2001).
21. K. Dieckmann *et al.*, *Phys. Rev. Lett.* **89**, 203201 (2002).
22. Z. Hadzibabic *et al.*, preprint available at http://arXiv.org/abs/cond-mat/0306050 (2003).
23. *S*-wave and *p*-wave interactions refer to two-body interactions with relative angular momentum 0 and $\hbar$, respectively.
24. M. Houbiers, H. T. C. Stoof, W. I. McAlexander, R. G. Hulet, *Phys. Rev. A.* **57**, R1497 (1998).
25. K. M. O'Hara *et al.*, *Phys. Rev. A.* **66**, 041401 (2002).
26. The transfer efficiency is limited by finite optical-trap depth and residual heating during the transfer.
27. K. Gibble, B. J. Verhaar, *Phys. Rev. A.* **52**, 3370 (1995).
28. For our modest degeneracy, we can use a Gaussian approximation for the density distribution. The mean density is then lower than the peak density by a factor of $2\sqrt{2}$.
29. Our estimate uses the direct mean field measurement of Bourdel *et al.* (*39*), scaled to our parameters.
30. C. Regal, D. S. Jin, preprint available at http://arXiv.org/abs/cond-mat/0302461 (2003).
31. Because of fermionic antisymmetry, there is no clock shift from interactions between atoms in states $|2\rangle$ and $|3\rangle$. Mean-field shifts arise only during a decoherence time (see later in the text) but are negligible if the population of atoms in state $|3\rangle$ is small.
32. E. G. M. van Kempen *et al.*, in preparation.
33. M. E. Gehm, S. L. Hemmer, S. R. Granade, K. M. O'Hara, J. E. Thomas, preprint available at http://arXiv.org/abs/cond-mat/0212499 (2002).
34. For fields higher than 630 G, number losses generally reduced n_1, and all the shifts in this region were scaled up by a factor of 1.1 to 2.7 but still remained negligible.
35. J. V. Steele, preprint available at http://arXiv.org/abs/nucl-th/0010066 (2000).
36. H. Heiselberg, *Phys. Rev. A.* **63**, 043606 (2001).
37. R. Combescot, preprint available at http://arXiv.org/abs/cond-mat/0302209 (2003).
38. K. M. O'Hara, S. L. Hemmer, M. E. Gehm, S. R. Granade, J. E. Thomas, *Science* **298**, 2179 (2002).
39. T. Bourdel *et al.*, preprint available at http://arXiv.org/abs/cond-mat/0303079 (2003).
40. This includes the recent measurement of 800 ± 40 G for the resonance in a_{12} (*39*).

41. The work at MIT was supported by NSF, the Office of Naval Research, the Army Research Office, and NASA. The work at Eindhoven is part of the research program of the Stichting voor Fundamenteel Onderzoek der Materie, which is financially supported by the Nederlandse Organisatie voor Wetenschappelijk Onderzoek.

4 April 2003; accepted 25 April 2003
Published online 8 May 2003;
10.1126/science.1085335
Include this information when citing this paper.

The Interface Phase and the Schottky Barrier for a Crystalline Dielectric on Silicon

R. A. McKee,[1]* F. J. Walker,[1,2] M. Buongiorno Nardelli,[1,3] W. A. Shelton,[1] G. M. Stocks[1]

The barrier height for electron exchange at a dielectric-semiconductor interface has long been interpreted in terms of Schottky's theory with modifications from gap states induced in the semiconductor by the bulk termination. Rather, we show with the structure specifics of heteroepitaxy that the electrostatic boundary conditions can be set in a distinct interface phase that acts as a "Coulomb buffer." This Coulomb buffer is tunable and will functionalize the barrier-height concept itself.

When Schottky (*1*) and Mott (*2*) formulated the barrier-height theory for a metal-semiconductor junction and later when Anderson (*3*) formulated the band-edge offset problem for semiconductor-semiconductor junctions, there was no consideration given to interface states as contributions to the electrostatic boundary conditions. The charge distribution at the interface was treated simply as a superposition of the bulk-terminated junction. Certainly these theories have been insightful, but they consistently misrepresent the barrier height or band-edge offsets because real interfaces, apparently from interfacial structure variations, modify the intrinsic band alignment (*4*–*6*).

Although the bulk-termination view of the problem has been enhanced over the years with an ever-increasing formalization of theoretical techniques (*7*–*15*), recent bond polarization ar-

[1]Oak Ridge National Laboratory, Oak Ridge, TN 37831, USA. [2]University of Tennessee (UT), Knoxville, TN 37996, USA. [3]North Carolina State University, Raleigh, NC 27695, USA.

*To whom correspondence should be addressed. E-mail: mckeera@ornl.gov